Continuously Welded Rail Longitudinal Resistance Modeling

Mohsen Amjadian, Ph.D.
Civil Engineering Department
The University of Texas Rio Grande Valley

Eleazar Marquez, Ph.D.
Mechanical Engineering Department
The University of Texas Rio Grande Valley

Arturo Fuentes, Ph.D.
Mechanical Engineering Department
The University of Texas Rio Grande Valley

Constantine Tarawneh, Ph.D.
Director, UTCRS
Mechanical Engineering Department
The University of Texas Rio Grande Valley

Jesus Amaro
Graduate Research Assistant
Civil Engineering Department
The University of Texas Rio Grande Valley

A Report on Research Sponsored by

University Transportation Center for Railway Safety (UTCRS)

The University of Texas Rio Grande Valley (UTRGV)

December 2025

Technical Report Documentation Page

1. Report No. UTCRS-UTRGV-I3CY24	2. Government Accession No.	3. Recipient's Catalog No.
4. Title and Subtitle Continuously Welded Rail Longitudinal Resistance Modeling		5. Report Date December 31, 2025
		6. Performing Organization Code UTCRS-UTRGV
7. Author(s) Mohsen Amjadian, Eleazar Marquez, Arturo Fuentes, Constantine Tarawneh, Jesus Amaro		8. Performing Organization Report No. UTCRS-UTRGV- I3CY24
9. Performing Organization Name and Address University Transportation Center for Railway Safety (UTCRS) The University of Texas Rio Grande Valley (UTRGV) 1201 W. University Dr. Edinburg, TX 78539		10. Work Unit No. (TRAIS)
		11. Contract or Grant No. 69A3552348340
12. Sponsoring Agency Name and Address U.S. Department of Transportation (USDOT) University Transportation Centers Program 1200 New Jersey Ave. SE Washington, DC, 20590		13. Type of Report and Period Covered Project Report June 1, 2024 - August 31, 2025
		14. Sponsoring Agency Code USDOT UTC Program
15. Supplementary Notes This work was a collaboration with MxV Rail		

16. Abstract

This research aimed to develop efficient 3D finite element (FE) models to simulate railroad longitudinal resistance in continuously welded rail (CWR). Using experimental data from the University Transportation Center for Railway Safety (UTCRS) and historical data from the Federal Railroad Administration's 1997 report on CWR behavior and a 2022 FRA-sponsored study on frozen ballast conditions, the goal of this study was to replicate and predict real-world force-displacement behavior in varying rail conditions. In this regard, a parametric FE model, which consists of a 600-ft rail segment and focuses on rail–tie interaction, was developed in ABAQUS software to simulate such conditions. In a conventional railroad system, the rail is the steel element that guides train wheels, ties are horizontal supports that hold the rails in place and transfer loads, and anchors are steel clamps that attach to the rail and bear against the tie to resist longitudinal movement. This modeling approach simulates the anchors as nonlinear springs based on experimental data, enabling better predictions in untested or challenging scenarios.

This project presented a unique opportunity, as UTCRS-UTRGV researchers have conducted relevant experimental work that could be directly utilized to inform and validate the finite element modeling, enhancing the accuracy and applicability of the results. The experimental setup involved a single rail segment approximately 26 inches in length mounted on a single tie with one anchor. A longitudinal load was applied to one side of the rail, while displacement was measured at the opposite end, allowing researchers to observe the railroad anchor resistance behavior under controlled conditions. These findings will aid in establishing anchor stiffness for future modeling of full rail resistance, including complex ballast conditions.

17. Key Words Finite element method; Longitudinal strength; Ground anchors; Continuous welded rail	18. Distribution Statement This report is available for download from http://railwaysafety.utrgv.edu/research/infrastructure/index.htm

19. Security Classification (of this report) None	20. Security Classification (of this page) None	21. No. of Pages 23	22. Price

Contents

List of Figures

List of Abbreviations and Terms

σ	Standard Deviation
BC	Boundary conditions
CWR	Continuously welded rail
DoF	Degrees of freedom
EA	Axial rigidity
ETA	Every tie anchored
FE	Finite element
FRA	Federal Railroad Administration
LVDT	Linear Variable Differential Transformer
PCHIP	Piecewise Cubic Hermite Interpolating Polynomial
P–u	Force–displacement relation
R^2	Coefficient of determination
RMSE	Root mean square error
RNT	Rail neutral temperature
TTCI	Transportation Technology Center, Inc. (Now MxV Rail)
UTCRS	University Transportation Center for Railway Center
UTRGV	The University of Texas Rio Grande Valley

Disclaimer

Acknowledgements

The authors wish to acknowledge the University Transportation Center for Railway Safety (UTCRS) for funding this project under the USDOT UTC Program Grant No 69A3552348340. The authors also wish to acknowledge engineer Stephen Wilk of MxV Rail for providing guidance throughout this project.

1. Introduction

1.1 Background

Continuously welded rail (CWR) is the widely adopted form of modern railroad track construction due to its reduced maintenance requirements, enhanced geometric stability, and ability to support higher operating speeds. The elimination of mechanical joints improves ride quality and reduces impact-driven deterioration. However, the continuity of CWR introduces significant thermally-induced longitudinal forces. Daily and seasonal temperature variations cause the rail temperature to deviate from the rail neutral temperature (RNT) and generate axial stresses. Elevated rail temperatures increase the risk of track buckling, while lower temperatures increase tensile loading as the rail contracts, promoting rail breaks and the formation of large gaps. The management of these risks depends on the longitudinal resistance provided by the coupled rail–tie–ballast system and the anchoring mechanisms that oppose axial motion [1] [2] [3].

RNT is the rail temperature at which the longitudinal thermal stress in a CWR is nominally zero (i.e., the "stress-free" state). The rail would freely expand or contract where the change in length is dictated by $\alpha L \Delta T$, where α is the coefficient of thermal expansion, L is the rail length, ΔT is the difference between the current temperature and the RNT. In CWR, this free movement is restrained, producing an axial force, N, on the order of $N \approx EA\alpha\Delta T$, where E is Young's modulus and A is cross-sectional area of the rail. The distribution of N along the track depends on the available longitudinal resistance. Both the absolute value of RNT and its spatial uniformity strongly influence buckle risk, gap formation, and the force distribution near discontinuities. RNT is a function of construction, maintenance history, environmental exposure, and the effective longitudinal stiffness provided by anchors and ballast. Accurate modeling of anchor resistance is therefore essential to predict how deviations from RNT are accommodated at both the specimen and system scales [2] [3].

1.2 Problem Statement:

Despite decades of study, widely used analytical and finite element (FE) models often rely on idealizations that compromise accuracy under challenging or atypical conditions. In particular, the contribution of anchor behavior is frequently represented with oversimplified, linearized surrogates that do not reflect the measured nonlinear force–displacement (P–u) response, nor do they capture variability across anchor types or ballast states (e.g., frozen or degraded). These limitations reduce the ability to expand simulation results beyond nominal conditions, compromising the confidence placed in computer simulations intended to inform maintenance strategy, RNT restoration, or break-response procedures [1] [2].

1.3 Research Objective

This study addresses those limitations by integrating experimental anchor stiffness values into a scalable FE framework. Laboratory tests conducted at the University Transportation Center for Railway Safety (UTCRS) at the University of Texas Rio Grande Valley (UTRGV), in collaboration with Federal Railroad Administration (FRA) datasets, provide the empirical foundation for constructing connector-based anchor representations calibrated to measured *P–u* behavior. Given the experimental data, anchors are modeled as nonlinear springs within the ABAQUS software to reproduce specimen-scale responses, and the resulting stiffness parameters are then implemented into a parametric 600-ft CWR model to analyze the system-level behavior under thermal loading. The objective is to provide a validated, experimentally-informed model capable of capturing anchor mechanics at the single rail–tie level. This model must remain computationally efficient and transferable to network-relevant lengths and conditions [1] [2].

2. Literature review

2.1 Previous Modeling Approaches

A notable effort in modeling CWR includes the work conducted by Transportation Technology Center, Inc. (TTCI), particularly their Longitudinal Resistance Modeling for Frozen Ballast study. This project developed a FE model to simulate rail break scenarios under frozen ballast conditions, which offered valuable insights into rail behavior under extreme environmental stress. However, the model served primarily as proof of concept and relied on generalizations, such as simplified boundary conditions and linear material behavior. These generalized assumptions constrained the applicability of the model in real-world engineering scenarios [1] [2].

2.2 Identified Gaps in Literature

Despite the contributions of previous studies, significant improvements are necessary in the modeling of longitudinal resistance. A missing component in the modeling aspect is the integration of experimental force-displacement data specific to different anchor types and ballast conditions. Many existing models treat anchor behavior as a static or idealized parameter, which fail to account for degradation, variation in installation, or environmental conditions such as freezing. This gap limits the use of such models in predictive maintenance and infrastructure design, particularly in climates prone to freeze–thaw cycles or in areas with mixed ballast compositions [1] [2] [3].

2.3 Contributions of the Present Study

This research addresses the aforementioned deficiencies by incorporating laboratory-measured anchor stiffness values into an experimentally-driven FE model. These values were obtained through controlled testing on a Track Panel Push Test (TPPT), as shown in Figure 1, conducted at the UTCRS. The TPPT measured the longitudinal resistance of various anchor configurations under load. By embedding these nonlinear characteristics into both 2D and 3D ABAQUS simulations, the study provides a higher-fidelity representation of anchor–tie–ballast interactions. This modeling approach allows for realistic simulations of CWR behavior under a broader spectrum of operational and environmental conditions and serves as a foundational step toward more reliable design practices and performance assessments in track engineering.

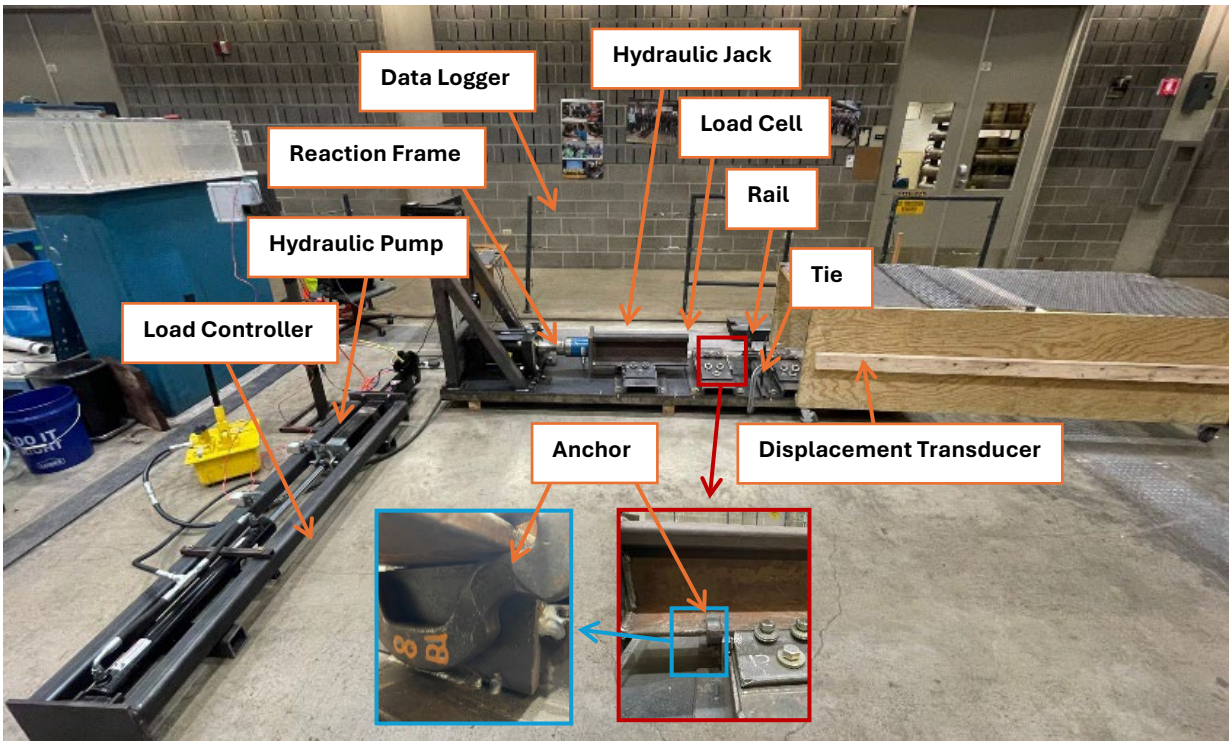

Figure 1. Photo of the UTRGV-UTCRS Track Panel Push Test (TPPT)

3. Methodology

3.1 Experimental Data Collection:

UTCRS conducted a TPPT to characterize rail–tie longitudinal resistance for three anchor types, labeled as anchors X Type, Y Type, and Z Type. Representative sketches of these anchors are shown in Figure 2. A 26-inch rail segment was mounted on a single timber tie with one anchor installed per test. An axial load was applied along the rail using a hydraulic jack reacting against a rigid frame and monitored by an inline load cell. As a result, longitudinal displacement was measured with a linear variable displacement transducer (LVDT) positioned at the opposite end of the rail and referenced to the tie, thereby capturing the rail–tie relative motion. The parameters recorded were the force and displacement via a National Instruments (NI) data acquisition (DAQ) system. Each anchor type was tested in 25 repeated trials under identical conditions.

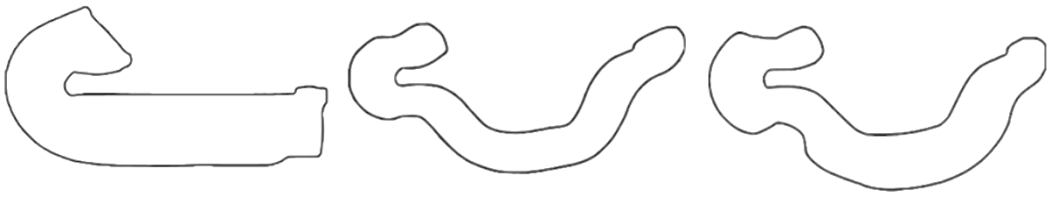

(a) X Type *(b) Y Type* *(c) Z Type*

Figure 2. Anchor types: (a) X Type, (b) Y Type, and (c) Z Type [4].

In the TPPT set up. the jack applies an axial load to the rail; while the transducer measures rail displacement relative to the tie. The resulting force–displacement records are used to calibrate the rail–tie interaction in the computer models.

3.2 Data Processing and Analysis:

Force–displacement records from the 25 push-test trials for each anchor family (X, Y, Z type) (Figure 3a–3c) were processed using MATLAB to obtain a representative calibration curve for the rail–tie interaction. For each trial, the measured load P (lb) was evaluated against displacement u (in) using a third-order polynomial (ordinary least squares), and the fitted relation was evaluated. To maintain physical plausibility near the origin, any negative predicted loads were truncated to zero and the curve was anchored at $(u,P) = (0,0)$. The representative P–u relation used for model calibration for a given anchor type was approximated by the pointwise median of the 25 interpolated curves; per-trial goodness–of–fit R^2 values were retained for traceability. Prior to implementation in ABAQUS, the representative median curve was converted to kips–inch units and exported as a tabulated pair set $\{u_i, P(u_i)\}$ for assignment to the axial response of the nonlinear connector elements.

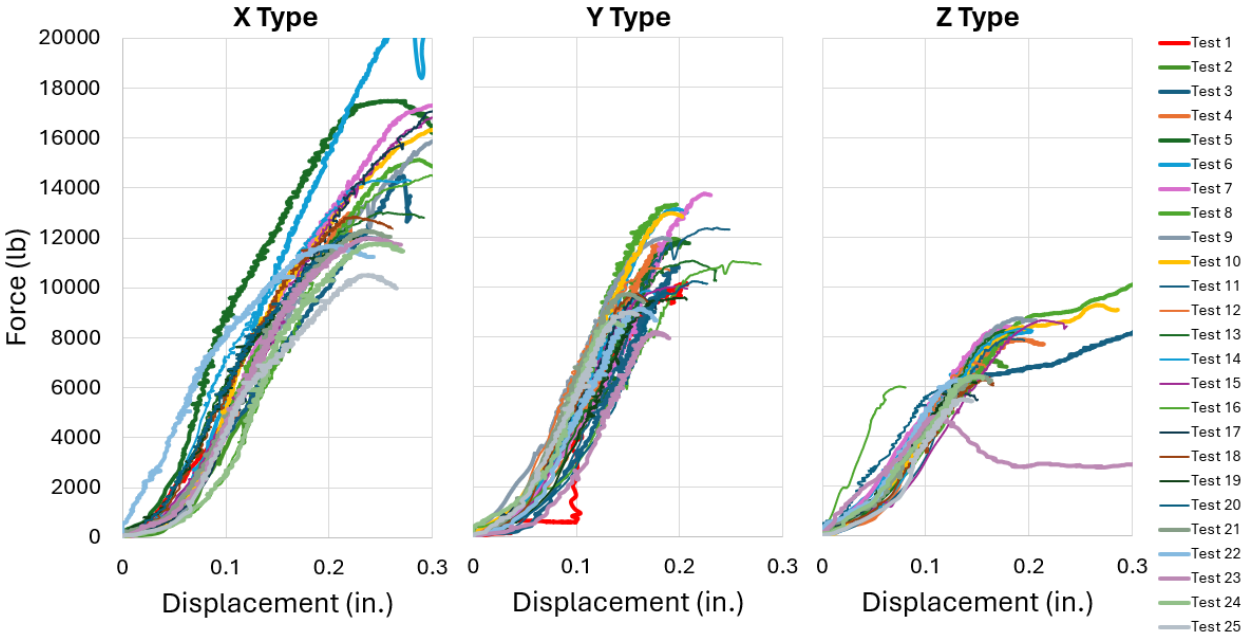

(a) *(b)* *(c)*

Figure 3. (a)X Type, (b)Y Type, (c)Z Type, the results for 25 experiments conducted for each anchor type [4].

3.3 Single Rail-Tie Model:

Figure 4a–4b illustrate the ABAQUS single rail–tie model constructed to reproduce the UTCRS laboratory configuration while isolating the rail–tie interaction. Figure 4a shows the meshed assembly; Figure 4b presents the same model with the rail lifted slightly from the tie to reveal the anchor representations. Anchors are implemented as nonlinear spring (connector) elements placed on either side of the rail foot and attached to the tie face nearest the applied load. The connector axial response is defined by the experimentally derived *P–u* relations (Section 3.2), thereby implementing measured anchor mechanics directly into the model.

Figure 5a–5b illustrate the loading conditions and restraints used to mirror the push-test protocol. Figure 5a applies the axial load as a distributed pressure over the rail end cross-section, consistent with laboratory actuation. Figure 5b shows the tie fixed at its base. No direct kinematic constraints are imposed on the rail beyond those necessary to suppress rigid-body modes, ensuring that longitudinal restraint arises from the calibrated connectors alone. This configuration captures the essential mechanics of the specimen and decouples the rail–tie longitudinal response from other effects (e.g., ballast).

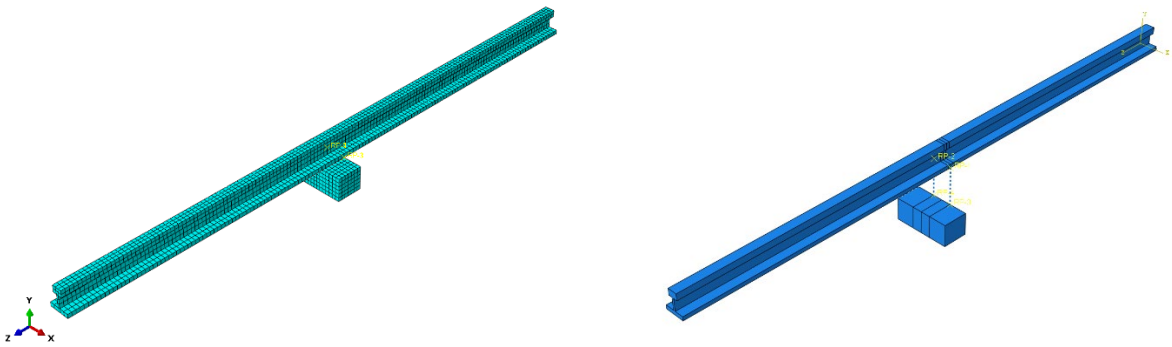

(a) *(b)*

Figure 4. ABAQUS finite element (FE) single rail-tie model. (a) Mesh of the rail–tie assembly. (b) Rail lifted to expose nonlinear spring (connector) elements

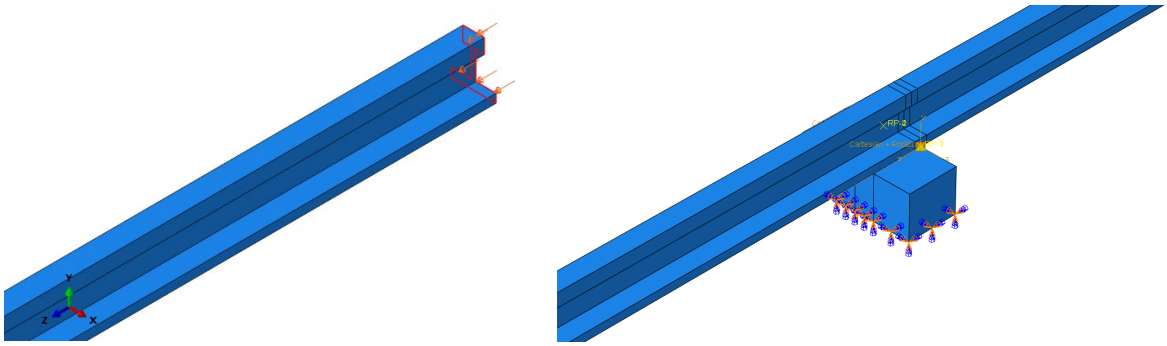

(a) *(b)*

Figure 5. FE boundary and loading conditions. (a) Axial loading applied as a distributed pressure over the rail end cross-section. (b) Tie fixed at the base.

Figure 6a–6c reports the input *P–u* curves used to parameterize the connectors for the X, Y, and Z Types (each averaged over 25 tests). These tabulated relations are the stiffness inputs governing rail–tie resistance in the model.

The input *P–u* curves are overlaid the corresponding 25 repeated tests to show that the selected curve provides representative average behavior for each anchor type. The goal of this specimen-scale model is to produce a simulated force–displacement response that closely matches the prescribed input for each anchor type, thereby confirming the implementation of the calibrated rail–tie interaction. The results of this agreement are presented in Section 4.1.

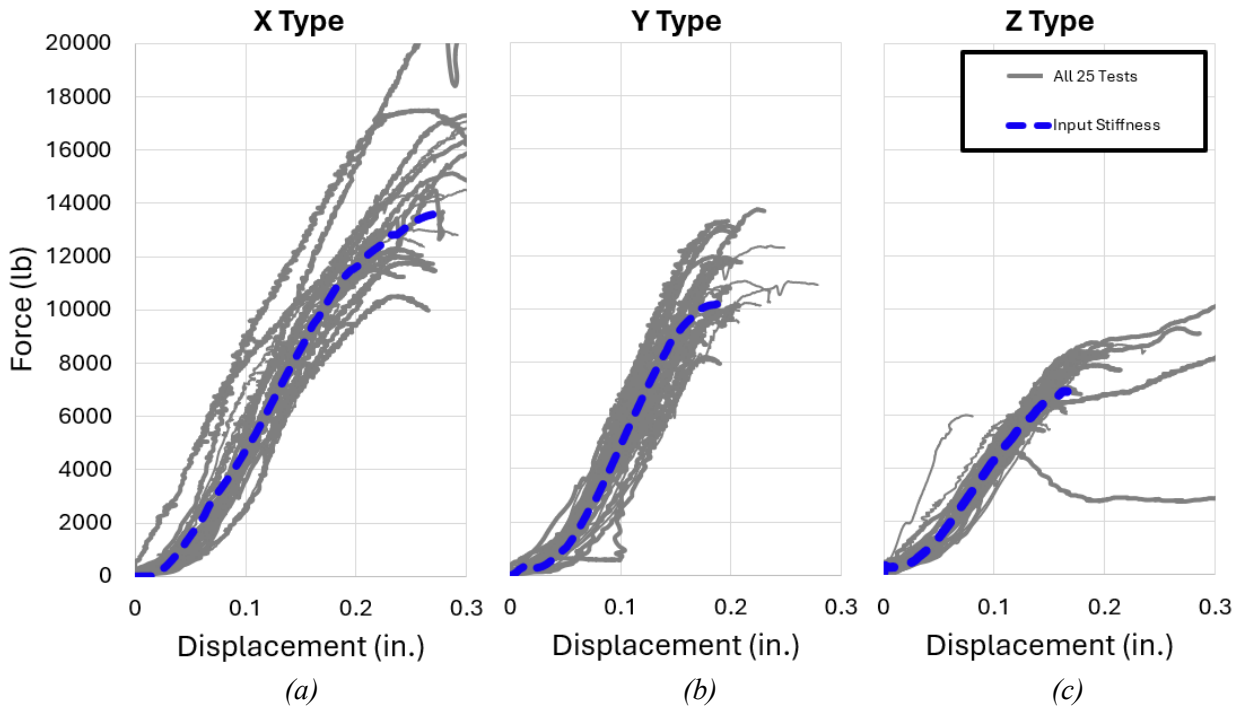

Figure 6. Input P–u curves for (a)X Type, (b)Y Type, (c)Z Type, and overlaid on the corresponding experimental force-displacement datasets.

3.4 600-ft Continuous Welded Rail Model:

A parametric three-dimensional model of a 600-ft continuously welded rail (CWR) segment was generated in ABAQUS via Python scripting. The rail and discrete timber ties are meshed consistently with the specimen model with ties placed at a uniform spacing of 19.5 inches, yielding approximately 369 supports over the span. The scripting framework generates the geometry, mesh density, connector placement, and material properties from a small set of inputs so that anchor properties, tie spacing, or loading can be changed without rebuilding the model.

The rail–tie interaction from the single rail–tie specimen is replicated at each tie location. The pair of nonlinear connector elements used to represent an anchor at the rail foot in the specimen model is replicated to every tie and attached to the tie face nearest the rail. Each axial response of the connector is defined by a tabulated force–displacement relation, which may be taken from the UTCRS-derived calibration (X, Y, and Z Types) or from a literature curve for validation exercises. In this way, the longitudinal resistance of the full system is the superposition of identical anchor interactions distributed at tie spacing. Figure 7 shows a parametric 600-ft CWR model with discrete ties at 19.5-in spacing.

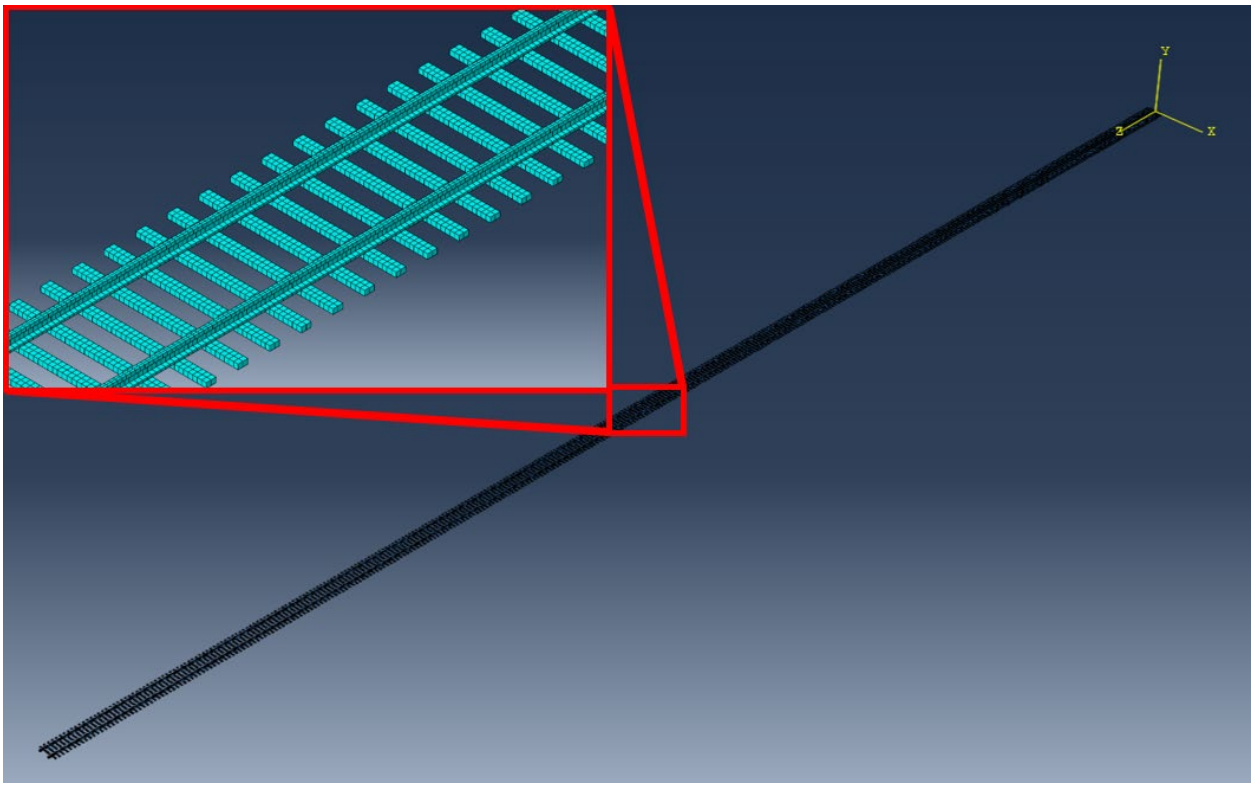

Figure 7. 600-ft continuous welded rail model.

To validate the system-scale formulation, the 600-ft CWR model was used under a uniform thermal drop from 80°F (26.7°C) to 10°F (-12.2°C) (ΔT = 70°F or 38.9°C) applied to the rail. The ties were held at their reference temperature. The anchor interaction at each tie was defined by the tri-linear *P–u* relation reported in *Longitudinal Resistance Modeling for Frozen Ballast*, assigned as the axial correlation of the connector elements and repeated at each tie at 19.5-in spacing. This produces a distributed longitudinal resistance consistent with the literature assumptions for frozen ballast conditions.

Ties are fixed at their bases. The rail is axially fixed at one end to represent continuity with the adjoining track, and axially free at the opposite end to represent a cut. No additional longitudinal restraints are imposed on the rail. Minimal constraints were used to suppress motion, similar to those shown in Figure 5. The load case is solved quasi-statically by ramping the temperature field to avoid inertial effects.

This model calculates the longitudinal displacement profile along the rail centerline, with particular attention to the free-end displacement and the decay length toward the fixed end. These predictions are compared to the system-level response for the same tri-linear anchor correlation from literature [1]. Such comparisons are presented in Section 4.2.

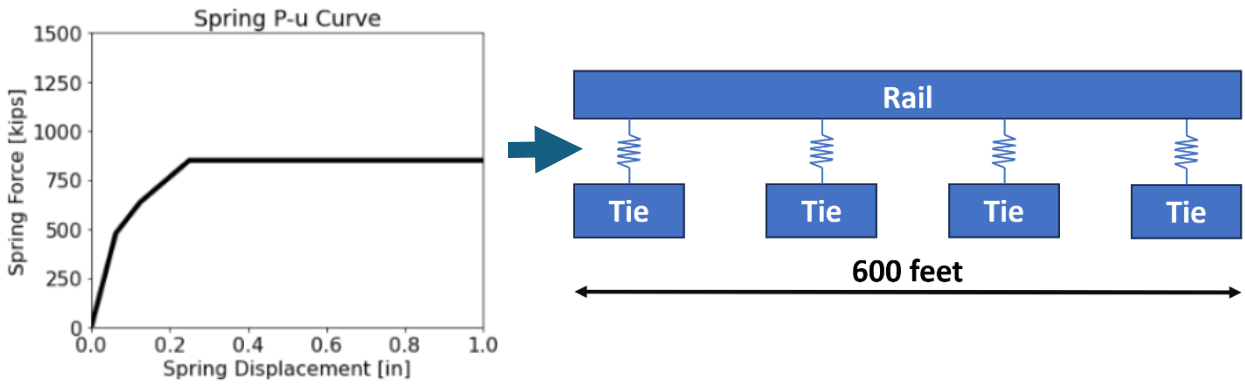

Figure 8. Validation setup for the 600-ft CWR model. Left: tri-linear anchor P–u curve adopted from the frozen-ballast study; right: schematic showing the correlation assigned to connector elements at each tie along the 600-ft rail [1].

4. Results

4.1 Single Rail-Tie Model:

4.1.1 Input stiffness vs. simulation

For anchor X, Y, and Z Types, the single rail–tie finite element model reproduced the prescribed input force-displacement (P–u) relations with near-complete overlap across the plotted range. The response reflected each characteristic signature of the anchors: X Type exhibited gradual nonlinear hardening; Y Type showed a steeper initial tangent stiffness indicative of early, firm engagement; and Z Type remained linear up to its threshold displacement. This alignment, shown in Figure 9a–9c, confirmed that the connector implementation accurately replicated the calibrated rail–tie interaction and that the specimen configuration isolated the longitudinal mechanism of interest.

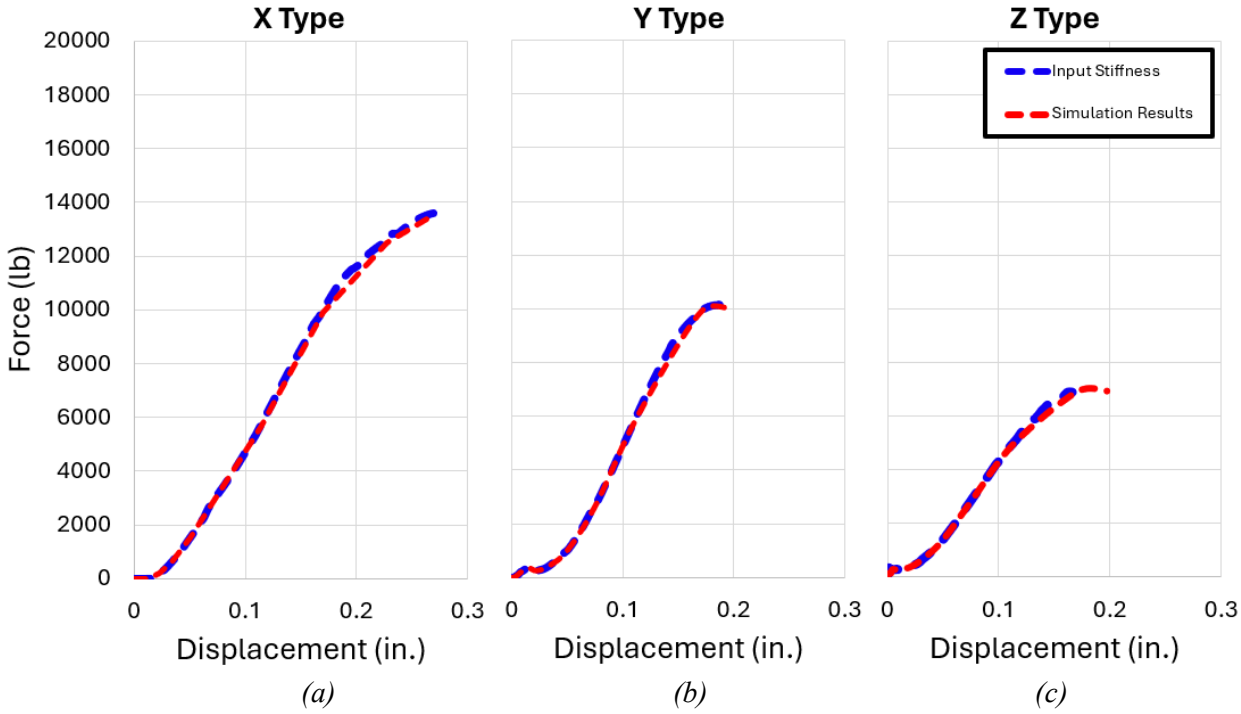

Figure 9. Comparison of the input P–u curves and single rail–tie simulation results for (a)X Type, (b)Y Type, (c)Z Type.

4.1.2 Agreement with repeated laboratory trials

When overlaid with the 25-trial experimental results, the simulated curves tracked the experimental mean within the observed scatter for all three anchor families. The correlation is most evident in the small-to-moderate displacement range that governs anchor engagement, shown in Figure 10a–10c.

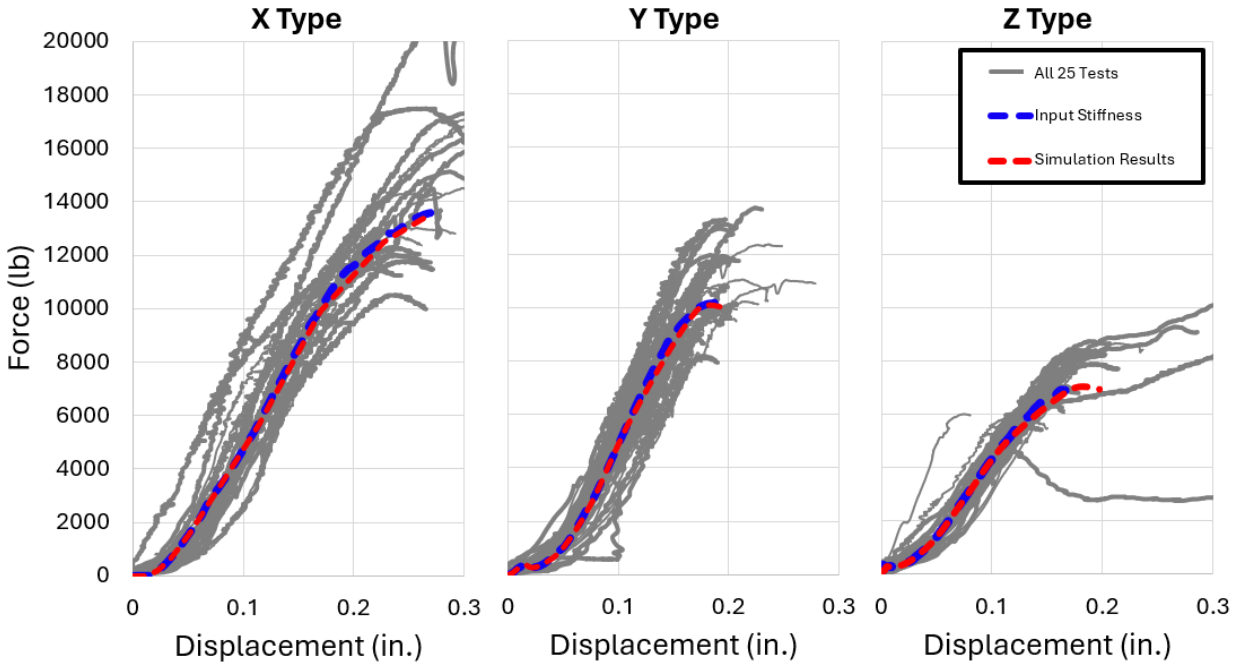

Figure 10. Comparison of input P–u stiffness, ABAQUS simulation response, and 25-test experimental results for (a)X Type, (b)Y Type, (c)Z Type.

4.2 600-ft Continuous Welded Rail Model:

4.2.1 Model Validation

Using the tri-linear anchor *P–u* relation described in *Longitudinal Resistance Modeling for Frozen Ballast*, the 600-ft simulation generated the displacement-along-the-rail curve reported in the literature. With the one-spring layer configuration, results closely match the benchmark in both the free-end displacement and the overall curve shape as displacement reduces from the free end toward the fixed end. This demonstrated that repeating the calibrated connector correlation at each tie provided a system response consistent with the frozen-ballast assumptions from literature [1].

A tie-spacing sensitivity analysis was conducted by modifying the spacing to 16 in and 24 in. The reduction in tie-spacing increased the total longitudinal restraint (greater anchor density per unit length), which produced a smaller free-end displacement and shorter influence length. Conversely, the increase in spacing produced a larger free-end displacement and extended the decay. Across the three spacings, the family of curves maintained the same functional form while varying in magnitude and decay rate, supports the robustness of the distributed-connector formulation.

Figure 11 shows the reference rail displacement after a cut. The one-spring layer configuration represents rail–tie interaction only. The two-spring layer configuration supplements rail–tie interaction with a tie–ballast spring fixed to ground, producing a slightly higher displacement curve than the one-spring

layer case. The current model corresponds to the one-spring layer configuration, and the results of the current model are shown in Figure 12. The next step is to incorporate the tie–ballast spring into the current model to replicate the two-spring layer result directly.

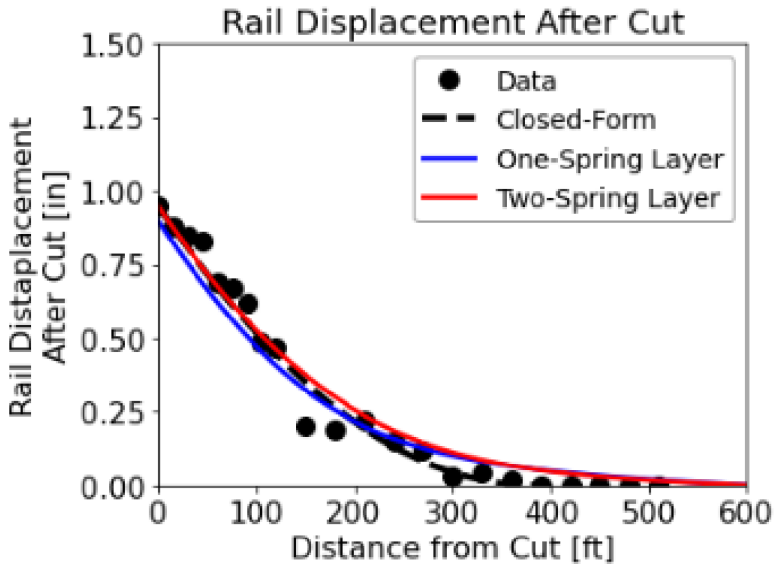

Figure 11. Reference result (frozen-ballast study): displacement along a 600-ft rail after a cut [1].

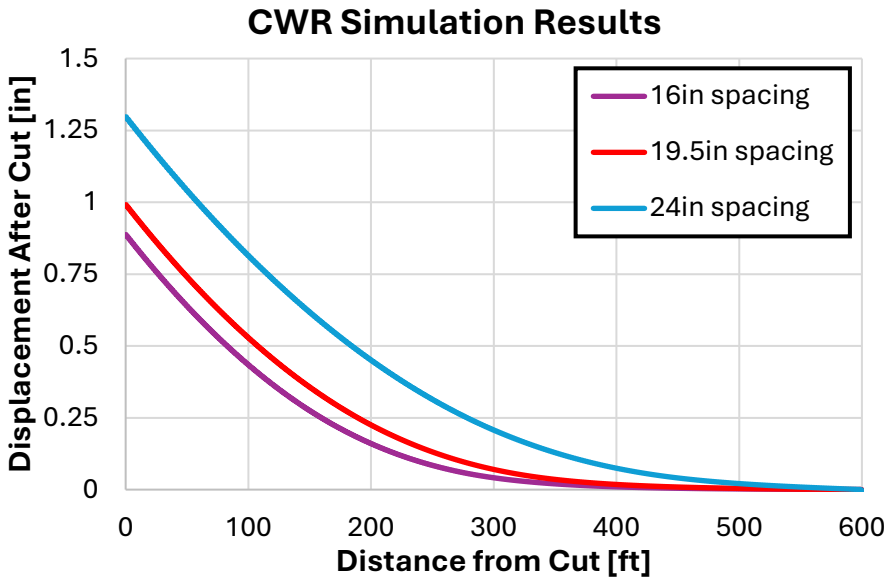

Figure 12. 600-ft CWR simulation results with tri-linear anchor correlation

4.2.2 Applying Experimental Data

Using the UTCRS-derived *P–u* relations for anchor X, Y, and Z Types (each averaged over 25 tests), the 600-ft model was run with 19.5-in tie spacing, ties fixed at their bases, the rail fixed at one end and free

at the other, and a uniform thermal drop from 80°F (26.7°C) to 10°F (-12.2°C). The resulting displacement-along-the-rail curves are shown in Figure 13. For all three anchor families, the free-end displacement is smaller and the entire curve lies below the validation baseline built from the assumed tri-linear stiffness [1]. The laboratory-measured anchors provide greater longitudinal resistance than the assumed curve used for the benchmark, so less axial movement is accommodated for the same thermal load. Differences between the X, Y, and Z Types reflect initial slope and nonlinearity of each anchor; the type with the higher initial tangent stiffness yields the lowest free-end displacement and the curve that drops toward near-zero displacement over a shorter distance from the cut.

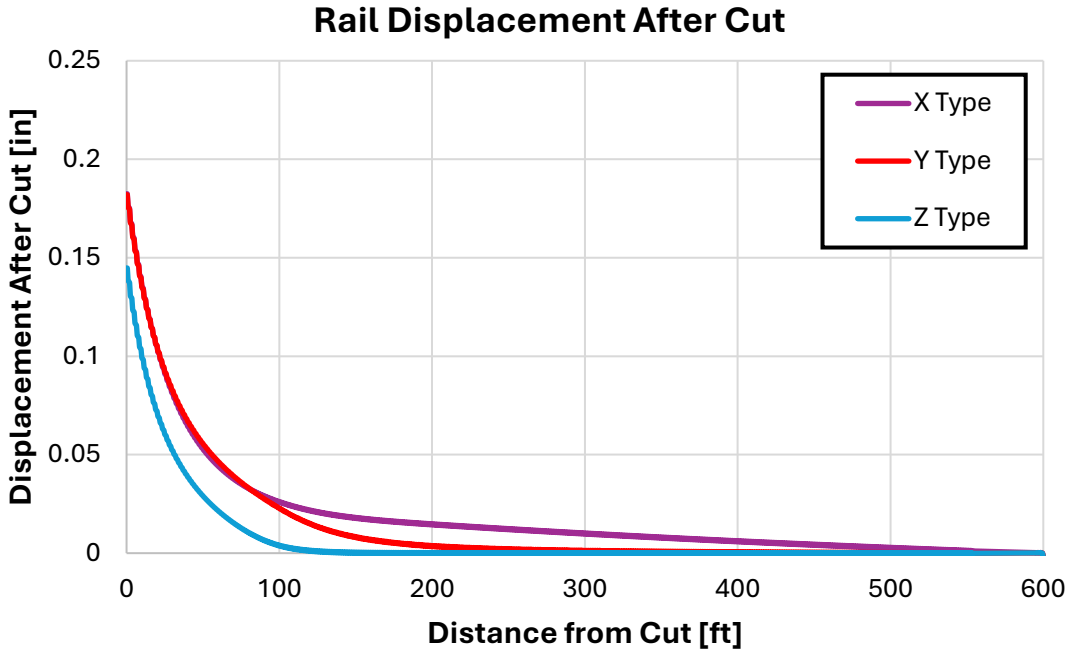

Figure 13. 600-ft CWR simulations using UTCRS anchor calibrations at 19.5-in tie spacing: (a) X Type, (b) Y Type, (c) Z Type. Curves show rail displacement versus distance from the cut.

The present configuration includes rail–tie interaction only (one-spring layer), these results are interpreted as an anchor-controlled lower bound on axial movement for a given thermal load and spacing. Incorporating a tie–ballast interaction (second-spring layer of the two-spring layer) is the natural next step and would shift the displacement–along the rail curve upward. The magnitude of this shift depends on the adopted ballast stiffness. To enable direct comparison with field data, the ballast spring can be calibrated to the FRA measurements referenced in the benchmark; thereafter, parametric runs can explore anchor density/spacing about 19.5-in, partial anchoring to represent missing or ineffective anchors, and thermal load envelopes (e.g., $\pm\Delta T$ scenarios) to bracket operational conditions.

5. Discussion

5.1 Fidelity of the anchor representation

The single rail–tie simulations, shown in Figure 9 and Figure 10, generate the experimentally derived *P–u* relations for the X, Y, and Z Types with near complete overlap, and when overlaid with the 25-trial results, track the experimental mean within the observed scatter. This confirms that modeling anchors as nonlinear connector elements calibrated from laboratory data is sufficient to capture the dominant rail–tie longitudinal resistance. The specimen configuration intentionally isolates this mechanism by excluding ballast effects and superfluous constraints, establishing a clean calibration step for system level analyses.

5.2 Transferability to system scale and alignment with the literature

Applying the calibrated anchor interaction at every tie in the 600-ft model (19.5-in spacing) yields displacement-along-the-rail curves consistent with the frozen-ballast benchmark when the same tri-linear anchor correlation is used, as shown in Figure 11 and Figure 12. When instead the UTCRS-measured correlations are applied, displayed in Figure 13, the curves lie below the benchmark, which is expected due to the measured anchors provide higher longitudinal stiffness than the assumed literature correlation. This coherence across scales indicates that the connector formulation is transferable. Parameters validated at the single rail–tie level carry through to system length without tuning.

5.3 What controls the curve: stiffness per unit length

The shape and level of the displacement-along-the-rail curve are governed by effective restraint per unit length. Two factors dominate: anchor correlation, and tie spacing. The higher initial or tangent stiffness in the anchor *P–u* lowers the curve and reduces the distance over which displacement becomes negligible. Tie spacing controls anchor density per unit length with closer spacing (e.g., 16-in vs. 19.5-in) increases restraint per unit length and lowers the curve; wider spacing (e.g., 24-in) reduces restraint and raises the curve.

These trends match a one-dimensional axial member on distributed support: increasing the effective stiffness per unit length reduces displacement levels everywhere along the rail.

5.4 Role of ballast representation

In the current one-spring layer configuration, ties are fixed at their bases, so longitudinal restraint is entirely anchor-controlled. Introducing an explicit tie-ballast spring converts each tie location into a series system (rail–tie–ballast), with equivalent per-tie stiffness.

Relative to the fixed-base surrogate, this reduces the effective restraint and shifts the displacement curve upward unless the ballast spring is very stiff. Calibrating the ballast spring to the FRA data from the benchmark study will enable direct replication of the two-spring layer result and a more realistic system baseline for frozen-ballast scenarios.

5.5 Connection to RNT and operational use

For a given structural configuration, changing $|T - RNT|$ scales the thermal driving force while the form of the displacement curve remains chiefly a function of restraint per unit length. This separation is operationally useful. RNT management governs the loading whereas anchor condition/density and ballast state govern the restraint. Consequently, interventions such as improving anchorage near anticipated discontinuities or tightening tie spacing locally can materially reduce axial movement for a given temperature excursion.

5.6 Limitations and scope

Interpretation is bounded by the single rail–tie calibration (single tie, single anchor per session), the lumped P–u description that captures local slip or seating, quasi-static loading without rate or cyclic degradation, and ensemble averaging without formal uncertainty propagation to system-scale predictions. Field measurements on instrumented track remain the definitive external validation.

5.7 Engineering takeaways and next steps

Anchor stiffness is first-order; accurate, type-specific calibration materially lowers displacement and should be prioritized in assessment and design. Tie spacing provides strong leverage, with modest changes around 19.5-in produce measurable differences, and targeted densification near potential cut locations is impactful offering practical mitigation strategy. Ballast modeling changes the baseline. Replacing a fixed tie base with a finite ballast spring raises displacement unless ballast stiffness is sufficiently high; calibrate to FRA data for frozen-ballast studies. The connector-based framework remains scalable and computationally efficient, enabling rapid parametric exploration of anchor type and density, tie spacing, ballast condition, thermal loading to support maintenance planning and break-response procedures.

Recommended next steps are to incorporate the tie–ballast layer and recalibrate against the FRA dataset, extending system-scale runs to X, Y and Z Types at 19.5-in spacing for a direct, three-type comparison, and add a light uncertainty analysis (e.g., ±1σ perturbations of the P–u correlation) to bracket expected ranges for free-end displacement and key waypoints along the rail.

6. Summary and Conclusion

In summary, the results demonstrate that experimentally calibrated nonlinear connector elements accurately reproduce the governing rail–tie longitudinal resistance at the specimen scale and transfer consistently to system-level without requiring additional empirical tuning. The longitudinal displacement profile along the rail is governed primarily by the effective restraint stiffness per unit length. Increased anchor stiffness and reduced tie spacing increase the distributed longitudinal resistance, resulting in lower displacement magnitudes and shorter influence lengths. Conversely, reduced anchor stiffness or wider tie spacing decreases the effective restraint density, producing higher displacements and longer decay lengths. The differences observed among X, Y, and Z type anchors directly reflect variations in their initial tangent stiffness and subsequent nonlinear hardening characteristics embedded within the calibrated *P–u* relations. The ballast representation materially sets the baseline response: in the current one-layer configuration (ties fixed at their bases) the behavior is anchor-controlled, whereas introducing an explicit tie–ballast spring placing anchor and ballast in series, reduces the equivalent per-tie stiffness relative to a fixed base, and consequently raises displacement unless the ballast is very stiff. Finally, the parametric 600-ft model offers an efficient platform for scenario analysis, varying anchor type, tie spacing, partial anchoring, and thermal loading, directly supporting RNT management, rail-break response planning, and maintenance decision-making.

The present calibration is based on a single-tie laboratory configuration and a lumped *P–u* description that approximates local slip and seating. Rate and cyclic effects were not modeled, and uncertainty from the experimental ensembles has not yet been propagated to system-scale predictions. Immediate extensions include adding a calibrated tie–ballast spring layer to replicate the two-spring layer literature result, repeating the system runs for all anchor types at 19.5-in for a direct three-type comparison, exploring partial anchoring and spatial variability, and performing field-scale validation. Incorporating basic uncertainty quantification around the *P–u* correlations will provide bounds on free-end displacement and key distances along the rail.

Overall, the results establish a practical, data-informed pathway for predicting longitudinal behavior in CWR. By tying model parameters to measured anchor mechanics and identifying stiffness per unit length as the primary control, the framework supports targeted interventions such as improving anchoring near anticipated discontinuities, adjusting spacing locally, and managing RNT. These measures can reduce axial movement under thermal loads and inform safer, more reliable operations.

References

[1] Baillargeon, J., Wilk, S., (2022). Longitudinal Resistance Modeling for Frozen Ballast. DOT/FRA/TTCI-22/07.

[2] Samavdem, G., Gomes, J., Kish, A., & Sluz, A. (1997). Investigation on CWR Longitudinal Restraint Behavior in Winter Rail Break and Summer Destressing Operations. DOT/FRA/ORD-97/01.

[3] Wilk, S. (2021). Ballast Parameters Influencing Lateral Track Resistance. Technology Digest, TD21-030(October). AAR/TTCI.

[4] Rahmaninezhad, S.M., Tarawneh, C., Fuentes, A., Vera, D. and Encinia, J., 2024. Rail Anchor Slip Force Testing (No. UTCRS-UTRGV-I6CY23). University Transportation Center for Railway Safety (UTCRS) Tier-1 University Transportation Center (UTC)